RSC Advances

PAPER

View Article Online
View Journal | View Issue

Cite this: *RSC Adv.*, 2022, **12**, 35270

Solvent-polarity reconfigurable fluorescent 4-piperazino-*N*-aryl-1,8-naphthalimide crown ether logic gates†

Gabriel Gauci and David C. Magri *

Four compounds **1–4** were designed and synthesised, comprising a 4-amino-*N*-aryl-1,8-naphthalimide fluorophore, a piperazine receptor, and an aryl group, as fluorescent logic gates. At the imide position, the substituent is phenyl (**1**), 1,2-dimethoxyphenyl (**2**), benzo-15-crown-5 (**3**), or benzo-18-crown-6 (**4**). Molecules **1** and **2** are constructed according to a fluorophore–spacer–receptor format, while **3** and **4** are engineered according to a receptor$_1$–spacer$_1$–fluorophore–spacer$_2$–receptor$_2$ format based on photoinduced electron transfer and internal charge transfer mechanisms. The compounds were studied in water, water/methanol mixtures of different ratios, and methanol by UV-visible absorption and steady-state fluorescence spectroscopy, as a function of pH, metal ions and solvent polarity. The excited state $p\beta^*_{H^+}$ of **1–4** is 8.4 ± 0.2 in water, 7.6 ± 0.1 in 1 : 1 (v/v) water/methanol, and 7.1 ± 0.3 in methanol. The $p\beta^*_{Na^+}$ of **3** in water is 0.92 and the $p\beta^*_{K^+}$ and $p\beta^*_{Ba^{2+}}$ of **4** in water are 2.3 and 2.9. ^{1}H NMR data in D_2O and CD_3OD confirm H^+ interaction at the piperazine moiety, and Na^+ and Ba^{2+} binding at the benzo-15-crown-5 and benzo-18-crown-6 moieties of **3** and **4**. By altering the solvent polarity, the fluorescent logic gates can be reconfigured between TRANSFER logic and AND logic. Molecules with polarity reconfigurable logic could be useful tools for probing the microenvironment of cellular membranes and protein interfaces.

Received 28th November 2022
Accepted 30th November 2022

DOI: 10.1039/d2ra07568g

rsc.li/rsc-advances

Introduction

The field of molecular logic-based computation[1] has attracted a considerable amount of attention since the inception of the first molecular AND logic gate in 1993 (ref. 2) based on photoinduced electron transfer (PET).[3] From these humble beginnings, the field has steadily moved forward from proof-of-concept demonstrations to potential societal applications.[4] Examples of fluorescent logic gates along these lines of exploration include multi-analyte AND logic gates (lab-on-a-molecules),[5] corrosion (Pourbaix) sensors,[6] medical diagnostics,[7] phototherapeutic releasing molecules,[8] tagging of micrometer objects,[9] cellular/enzyme monitoring[10] and edge detection.[11]

The first molecular AND logic gates by de Silva were studied in alcohol solutions of methanol and propanol.[2,12] Methanol is the *de facto* solvent substitute for water when solubility is an issue, while ethanol is a less toxic alternative for cellular studies.[13] In many studies, a compromise is to use water/alcohol solvent compositions.[14] Given this tendency, it is often assumed that the alcohol/water ratio readily correlates to the fluorescence quantum yield (Φ_F). However, to the best of our knowledge, there are no systematic studies that examine the effect of solvent polarity, specifically in water/methanol, on the photophysical parameters of crown ether sensors (*i.e.* Φ_F).[15] In biological systems, notably at the cellular level, polarity determines interactions with proteins and enzymes, and the permeability of membrane compartments.[16] Evidence suggests that mitochondrial[16] and lysosomal[17] polarity in cancer cells is lower than in normal cells. And so a better understanding of polarity effects is medicinally useful.

Crown ether-based chemosensors, although dating over three decades, still attract attention.[18–20] Recently, there is considerable interest in PET chemosensors for Ba^{2+}.[21] Physicists are searching for evidence that neutrinos are their own anti-particles by investigating neutrinoless double beta decay of ^{136}Xe to $^{136}Ba^{2+}$.[22] Using single molecule fluorescent imaging (SMFI), experimentalists are searching for Ba^{2+} *in situ* and in real time from the decay of ^{136}Xe in high pressure xenon gas under ultra-vacuum conditions. Thapa and co-workers have reported diazacrown 4-amino-1,8-naphthalimide chemosensors for Ba^{2+} in acetonitrile and in dry phase.[23] In this study, as with many azacrown chemosensor studies, acetonitrile is used as the solvent. There is a tendency for trace water and/or hydrated metal ions to act as unsuspecting proton sources.[24] Hence, the emission enhancement may not always be due to metal ion

Department of Chemistry, Faculty of Science, University of Malta, Msida, MSD 2080, Malta. E-mail: david.magri@um.edu.mt

† Electronic supplementary information (ESI) available: Experimental details, UV-vis absorption, emission, NMR, IR and mass spectra. See DOI: https://doi.org/10.1039/d2ra07568g

complexation, but rather to protonation of a nitrogen atom. A remedy to this issue is to use oxacrown ethers.[25]

In our previous study, we investigated the properties of 4-methylpiperazino-*N*-aryl-1,8-naphthalimides.[26] We discovered that a carbonyl moiety of the 4-piperazino-1,8-naphthalimide fluorophore assists in metal ion binding (*i.e.* Na^+, K^+) within the benzo-15-crown-5 and benzo-18-crown-6 cavities in the excited state. Building upon this finding, we have investigated 4-piperazino-*N*-aryl-1,8-naphthalimides with benzo-15-crown-5 and benzo-18-crown-6 moieties as solvent-polarity reconfigurable logic gates. We selected piperazine as the proton receptor, which is readily protonated in neutral water, to facilitate ^{1}H NMR titration experiments in D_2O. An objective was to examine whether there is any ground state interaction between a carbonyl of the naphthalimide and the metal ion within the crown cavity.[26] We have also systematically and thoroughly examined the effect of water/methanol solvent compositions in 10% (v/v) increments on the photophysical properties of four 4-amino-*N*-aryl-1,8-naphthalimide logic gates. Molecules **3** and **4** are designed with a receptor$_1$–spacer$_1$–fluorophore–spacer$_2$–receptor$_2$ format[12] based on PET[3] and internal charge transfer (ICT) with a 1,8-naphthalimide fluorophore, a piperazine moiety at the 4-position and a benzocrown ether at the imide position. Spacer$_1$ is the *N*-imide node, and spacer$_2$ is the diethylene bridges within the piperazine moiety consistent with C_0-type and C_2-type spacers.[27] Molecules **1** and **2** with phenyl and 1,2-dimethoxyphenyl moieties serve as fluorophore–spacer–receptor models (Scheme 1).

Results and discussion

The syntheses of **1–4** are shown in Scheme 1. 4-Chloro-1,8-naphthalic anhydride was reacted with aniline, 3,4-dimethoxyaniline, 4′-aminobenzo-15-crown-5 or 4′-aminobenzo-18-crown-6.[16] The 4-chloro-*N*-aryl-1,8-naphthalimides were then reacted with excess piperazine in *N*,*N*-dimethylformamide (DMF) at 130 °C. The products were recovered as orange powders in good yields ranging from 77–94% after precipitation from a suitable solvent. The compounds were characterised by standard spectroscopic techniques including ^{1}H, ^{13}C, and ^{13}C DEPT-135 NMR, FTIR, and HRMS. Full details are provided in the Experimental section. The corresponding spectra are available in the ESI (Fig. S1–S16†).

The thermodynamic driving forces for PET, based on the Weller equation (eqn (1)) from the piperazine secondary amine and the 3,4-dimethoxyphenyl to the excited state amino-1,8-naphthalimide fluorophore, are 0.07 eV and 0.37 eV (6.7 kJ mol^{-1} and 35 kJ mol^{-1}).[28]

$$\Delta G_{PET} = E_{ox} + E_{red} - E_S - e^2/\varepsilon r \quad (1)$$

These estimates are based on known electrochemical data.[12,28] Although the values are mildly endothermic, they are influenced by the solvent polarity according to the coulombic term $e^2/\varepsilon r$, where ε is the solvent dielectric constant. Intramolecular PET in neutral molecules generates a charged radical ion pair, which is stabilised by solvents with dipole moments. Generally, the greater the solvent polarity, the more stabilised the radical ion pair resulting from PET, and so the Φ_F falls concurrently.[25,26] As part of this study, we have systematically examined the effect of the ε (methanol: 33, water: 80) on the competition between PET and fluorescence as a continuum between water to methanol in 10% (v/v) methanol increments.

The UV-visible absorption spectra of **1–4** were first examined as a function of acidity in water, 1 : 1 (v/v) water/methanol, and methanol (Fig. S17–S20).† A summary of data for **1–4** is available in Table S1† and specifically for **4** in Table 1. Compounds **1** and **2** have λ_{max} at 405 nm and 403 nm in water. In 10^{-4} M H^+, slight hypsochromic shifts of 8 nm and 2 nm are observed. The log ε of **1** and **2** are 3.18 ± 0.05 and 3.54 ± 0.04 and are indicative of $\pi \rightarrow \pi^*$ transitions. In methanol, the λ_{max} is 393 nm for **1** and **2**. Overall, there is little change in the UV-vis spectra of **1** and **2**, with the exception of **1** in water with an isosbestic point at 345 nm. In 1 : 1 (v/v) water/methanol and methanol, the log ε for **1–4** are relatively constant at 3.98 ± 0.11. The spectra of **3** are generally consistent with H^+-induced peak shifts of 14 nm,

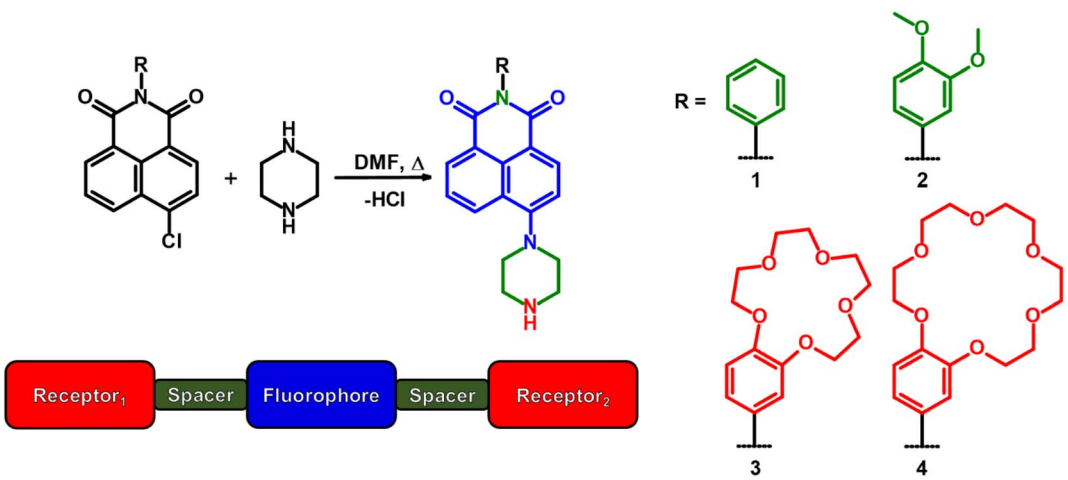

Scheme 1 The synthesis of 4-piperazino-*N*-aryl-1,8-naphthalimide molecular logic gates **1–4** and the design format of **3** and **4**.

10 nm and 6 nm in water, 1 : 1 (v/v) water/methanol and methanol, respectively, with isosbestic points at 416 nm, 409 nm and 402 nm. In contrast, the spectra of **4** are notable. Titrations of **4** from 10^{-11} M to 10^{-4} M H^+ reveals bathochromic shifts of 14 nm, 24 nm and 21 nm accompanied by hyperchromic shifts with a λ_{max} at 392 nm, 389 nm and 380 nm in water, 1 : 1 (v/v) water/methanol and methanol, respectively. Isosbestic points appear at 416 nm, 409 nm and 402 nm. Isosbestic points are distinctly observed in all three composition solvents for **3** and **4** (and for **1** in water).

An analysis of the absorbance–pH plots provided ground state proton binding constants (pK_a, $p\beta_{H^+}$) (Fig. S21–S24†). For **1** in water, and **3** and **4** in all solvent compositions (Fig. S17a, S19 and S20†), significant changes occur in the absorbance maxima upon protonation. In the three solvents, the spectra of **4** (and **1** in water) exhibits simultaneous changes to the absorbance and wavelength. These observations are consistent with a twisted ICT (TICT) state due to charge repulsion and a geometry change on protonation of the piperazine.[29] The spectra of **2** shows no such changes, while with **3** only a slight change in the wavelength is observed.

The emission properties of **1–4** (Fig. S25–S28†) as a function of acidity are tabulated (Tables 1 and S1†). The λ_{max} in water at 10^{-4} M H^+ of **1–4** appear between 540 nm and 549 nm. In methanol, the λ_{max} is red-shifted by 8 nm to 20 nm. H^+-induced Stokes shifts of *ca.* 140 nm (71 429 cm^{-1}) occur. The Φ_F in acid ranges between 2% and 7%, and in base from 0.2% to 3%. Clear digital off–on switching across the solvent polarity continuum is identified with **4** between 10^{-11} M H^+ (vial B) and 10^{-4} M H^+ (vial A). Irradiated with a 365 nm UV lamp, acidic solutions of **4** emit yellow light in water and green light in methanol (Fig. 1).

Fig. 2 shows the fluorescence spectra of **4** in water as a function of (a) H^+, (b) Ba^{2+} and (c) water/methanol solvent composition. Titration with acid from 10^{-11} M H^+ to 10^{-4} M H^+ results in a fluorescence enhancement (FE) of 72 with a peak maximum at 540 nm. The emission increases due to protonation of the piperazine nitrogen atom, which inhibits the TICT from the lone pairs of the aliphatic nitrogen atom to the fluorophore.[5,29] Titration with Ba^{2+} in 10^{-4} M H^+ results in a further emission increase due to complexation of Ba^{2+} within the crown cavity (Fig. 2b), which raises the oxidation potential E_{ox} of the benzocrown and consequently raises ΔG_{PET} so that PET from the benzocrown to the 4-aminonaphthalimide is prevented. We also observe in Fig. 2c, counterintuitively and unlike **1–3** (Table S1†), an increase in the emission (and Φ_F, Table 1) of **4** on changing the solvent from methanol to water. Being a $\pi \rightarrow \pi^*$ transition, we naturally expect the carbonyl oxygen atoms to be more basic in the excited ICT state than in the ground state.[14] This observation suggests that **4** is less strongly hydrogen bonded at a carbonyl oxygen in the excited state than in the ground state, perhaps due to a conformational change associated with the more flexible and bulky ethoxy linkages within the benzo-18-crown-6, which alters the solvent shell.

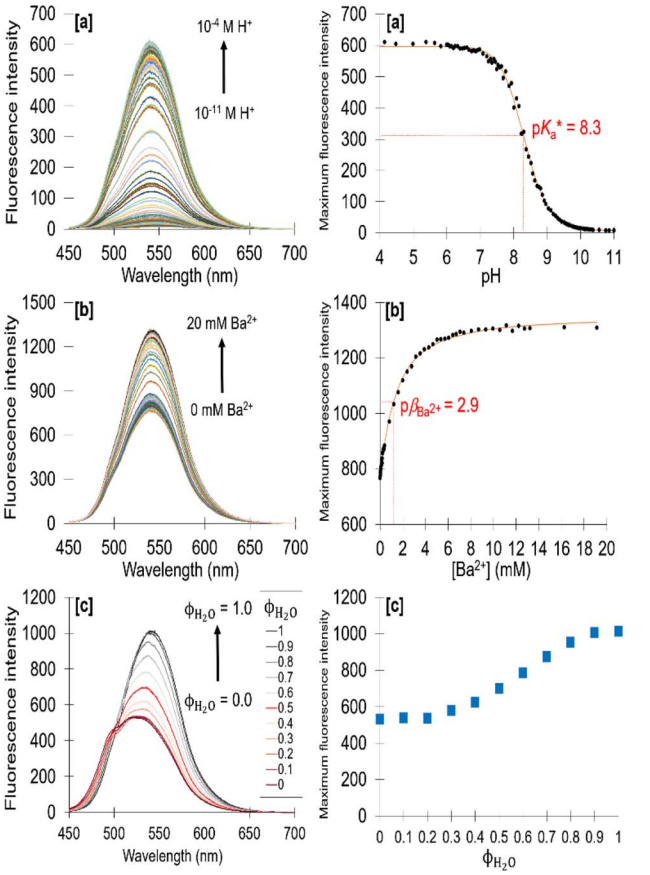

Fig. 2 Emission spectra in water of 14 μM **4** as a function of (a) H^+, (b) Ba^{2+} at 10^{-4} M H^+, and (c) methanol/water solvent compositions at 10^{-4} M H^+, and the intensity–concentration profiles. λ_{ex} = 400 nm.

From the fluorescence titrations of **1–4**, the excited state proton binding constants (K_a^*, $\beta_{H^+}^*$) and cation binding constants ($\beta_{M^+}^*$) were evaluated. The binding constant is defined as the concentration at which half of a receptor is occupied by the specific analyte. Proton binding constants were determined from absorbance (eqn (2)) and

$$A = \frac{A_{max} \times 10^{(pH-pK_a)} + A_{min}}{1 + 10^{(pH-pK_a)}} \quad (2)$$

$$I_F = \frac{I_{F,max} \times 10^{(pH-pK_a^*)} + I_{F,min}}{1 + 10^{(pH-pK_a^*)}} \quad (3)$$

fluorescence (eqn (3)) intensity plots using Henderson–Hasselbalch equations, which produce a sigmoidal titration curve.[30]

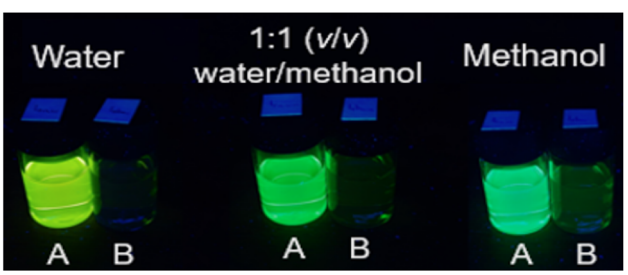

Fig. 1 Molecule **4** irradiated with 365 nm light in water, 1 : 1 (v/v) water/methanol and methanol with 10^{-4} M H^+ (vials A) and 10^{-11} M H^+ (vials B).

The analyte-intensity data was fitted as a non-linear equation, and the binding constants were obtained from the point of inflection (Fig. S29–S32†) where I_F, $I_{F,max}$ and $I_{F,min}$ are the observed, maximum and minimum fluorescence intensities. A similar equation was used to calculate the metal cation binding constants $\beta^*_{M^+}$ with the benzocrown ethers.[25] The $p\beta^*_{H^+}$ of **1–4** are 8.4 ± 0.2 in water, 7.6 ± 0.1 in 1 : 1 (v/v) water/methanol and 7.1 ± 0.3 in methanol. The $p\beta^*_{Na^+}$ of **3** is 0.92 in water and 1.4 in 1 : 1 (v/v) water/methanol (Fig. S33–S35†). These values are greater those of anthracene-based logic gates.[2,12] The $p\beta^*_{Ba^{2+}}$ of **4** in water is 2.9 (Fig. S36–S38†) and 3.7 in 1 : 1 (v/v) water/methanol (Fig. S39–S41†). No evidence for metal ion binding was observed with **2** bearing the 3,4-dimethoxyphenyl moiety.

Molecules **3** and **4** displays logic characteristics dependent on the solvent conditions (Fig. S42† and 3). The threshold limit is set at half of the maximum fluorescence of the most intense emission spectrum (1, 1). In water, **3** and **4** behave as single-input H^+-driven YES gates. When Na^+ and Ba^{2+}, respectively, are included as inputs in water, **3** and **4** function as a two-input H^+, M^+-driven TRANSFER logic gates (Fig. S42a† and 3a). A third cation, such as K^+ or Hg^{2+} ($p\beta_{K^+} = 2.3$, $p\beta_{Hg^{2+}} = 3.4$ in water, Fig. S36–S38†) can also bind within the benzo-18-crown-6 cavity to yield an integrated OR–AND gate algebraically expressed as (A + B)·C.[1a]

In methanol, **4** functions as a two-input H^+, Ba^{2+}-driven AND logic gate (Fig. 3b) and **3** as a two-input H^+, Na^+-driven AND gate (Fig. S42b†). At high H^+ and Ba^{2+} levels, the emission of **4** is high with a Φ_F of 0.153 and a switching ratio of 51. For comparison, **3** has a high Φ_F of 0.163 and turn-on ratio of 9 at high H^+ and Na^+ levels. This tale of two solvents is an example of logic function tuning by solvent polarity.[15,31] Rather interestingly, the optimal Φ_F of **3** is observed in methanol while for **4** it is observed in 1 : 4 (v/v) water/methanol (Fig. 4), the latter with a 5-fold emission enhancement. The addition of water to **3** in the presence of H^+ and Na^+ in pure methanol causes a clear decreasing trend in the Φ_F output (Fig. 4, × symbol). However, in the case of **4** in the presence of H^+ and Ba^{2+}, an increase of up to 20% water in methanol enhances the Φ_F output, which on further addition of water, then causes a decrease in the Φ_F output (Fig. 4, ■ symbol). Labelled with respect to the volume fraction of water, the *x*-axis of Fig. 4 is also indicative of the dielectric constant ε ranging from 33 to 80 for methanol and water, respectively. The general trend is that the Φ_F decreases with increasing ε.

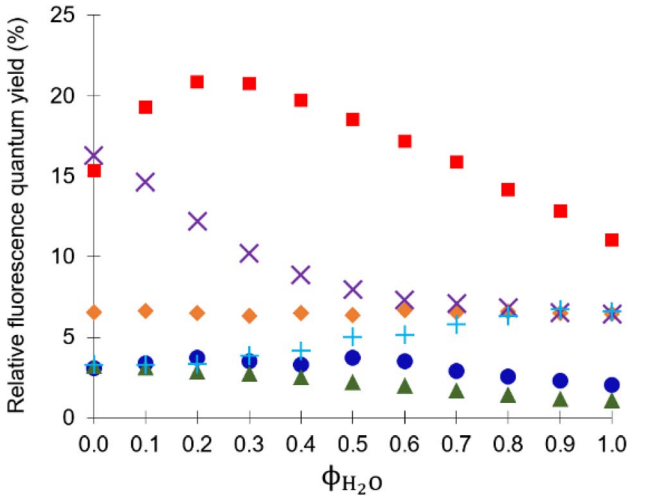

Fig. 4 Fluorescence quantum yields (Φ_F) in different water/methanol solvent compositions as a water volume fraction at 10^{-4} M H^+ for (●) 9 μM **1**-H^+, (▲) 10 μM **2**-H^+, (♦) 9 μM **3**-H^+, (x) 9 μM **3**-H^+ and 10^{-2} M Na^+, (+) 14 μM **4**-H^+, and (■) 14 μM **4**-H^+ and 10^{-2} M Ba^{2+}.

^{1}H NMR study

^{1}H NMR spectra were examined as a function of pD and either pNa or pBa for **3** and **4** in CD_3OD (Fig. S47† and 5) and D_2O (Fig. S43 and S45†).[32] Fig. 5 and S47† show the ^{1}H NMR spectra of **3** and **4** in CD_3OD as 'truth-table' studies under four input conditions. In D_2O **3** was not fully soluble without acid so only two states were examined (Fig. S45†), while **4** was soluble for all four conditions. We alert the reader to the fact that the NMR measurements are ground state measurements, so any effect of D^+, OD^-, Na^+ and Ba^{2+} is not directly comparable to the emission results. Generally, the ^{1}H NMR spectra can be qualitatively divided into three regions. As illustrated in Fig. 5a, between 6.9 ppm and 8.7 ppm, there are sharp signals attributed to the five naphthalimide protons (H_1–H_5) at 7.4–8.7 ppm, and the three

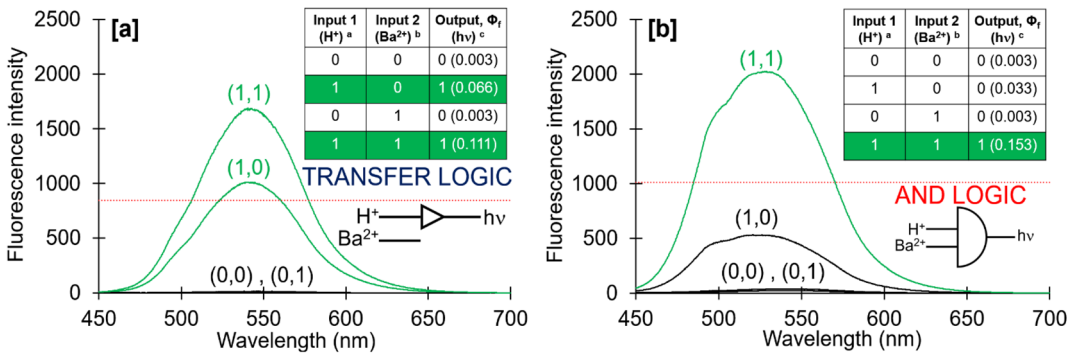

Fig. 3 Fluorescence emission spectra of 14 μM **4** in (a) water and (b) methanol. The red line denotes the digital threshold, which was set at $\Phi_{F,max}$/2. [a] Low input: 10^{-11} M H^+, high input: 10^{-4} M H^+; [b] low input: 0 mM Ba^{2+}, high input: 14 mM Ba^{2+}; [c] measured with reference to quinine hemisulfate in 0.1 M H_2SO_4.

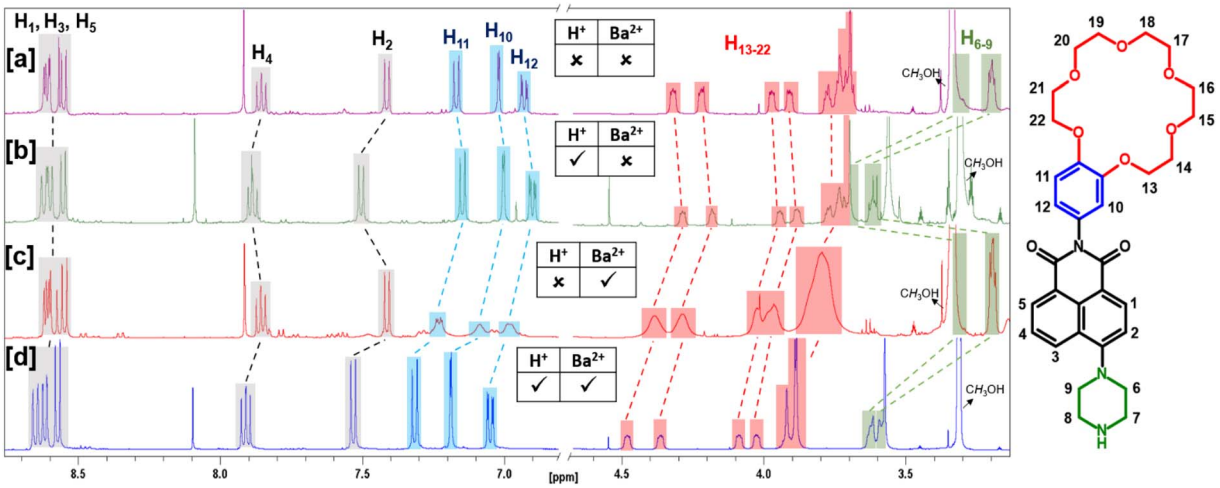

Fig. 5 ^{1}H NMR spectra of 8 mM **4** in CD_3OD: (a) 50 mM NaOD added, (b) 50 mM DCl added, (c) 50 mM NaOD and 85 mM Ba^{2+} added, and (d) 50 mM DCl and 85 mM Ba^{2+} added.

Table 1 Spectroscopic parameters of **4** in water, 1 : 1 (v/v) water/methanol and methanol.[a] See Table S1 in the ESI for **1–3**

Parameter	H_2O ($\phi_{H_2O} = 1.0$)	H_2O/MeOH ($\phi_{H_2O} = 0.5$)	MeOH ($\phi_{H_2O} = 0.0$)
$\lambda_{abs,\ 10^{-4}\ M\ H^+}$/nm	392	389	380
Log $\varepsilon_{10^{-4}\ M\ H^+}$[b]	3.49	4.03	4.05
$\lambda_{abs,\ 10^{-11}\ M\ H^+}$/nm	406	413	401
Log $\varepsilon_{10^{-11}\ M\ H^+}$[b]	3.38	3.94	3.97
λ_{iso}/nm	336, 409	321, 405	315, 394
$\lambda_{em,\ 10^{-4}\ M\ H^+}$/nm[c]	540	536	520
$\Delta\lambda_{10^{-4}\ M\ H^+}$/nm[d]	148	147	140
$\Delta\nu_{10^{-4}\ M\ H^+}$/cm^{-1}[e]	67 568	68 027	71 429
$\Phi_{F,\ 10^{-4}\ M\ H^+}$[f]	0.066	0.050	0.036
$\Phi_{F,\ 10^{-11}\ M\ H^+}$[f]	0.002	0.002	0.002
FE[g]	72	22	13
pK_a[h]	8.6	7.5	7.1
pK_a^*[i]	8.3	7.5	7.0

[a] 10^{-4} M. [b] ε in L mol^{-1} cm^{-1}. [c] $\lambda_{ex} = 400$ nm. [d] $\Delta\lambda = \lambda_{em} - \lambda_{abs}$. [e] $\Delta\nu = 1/\lambda_{abs} - 1/\lambda_{em}$. [f] Measured with reference to quinine hemisulfate in 0.1 M H_2SO_4. [g] Proton-induced fluorescence enhancement, $I_{F_{10^{-4}\ M\ H^+}}/I_{F_{10^{-11}\ M\ H^+}}$. [h] Determined by eqn (2). [i] Determined by eqn (3).

phenyl protons (H_{10}–H_{12}) at 6.9–7.4 ppm. The multiplets at 3.7–4.5 ppm are due to the benzocrown (H_{13}–H_{22}) and those at 3.4–3.5 ppm are due to the piperazine (H_6–H_9).

The uppermost ^{1}H NMR spectrum of **4** in CD_3OD (Fig. 5a) was recorded in the presence of NaOD to ensure that the logic gate was unprotonated. The five naphthalimide protons appear at 7.4 ppm and 7.8 ppm as a doublet and apparent triplet, and as a superimposed cluster of three resonances at 8.5–8.7 ppm. The three phenyl protons are resolved as three multiplets at 6.8–7.2 ppm. On protonation of **4** to **4**-D^+ (Fig. 5b) in CD_3OD, there is a large $\Delta\delta_H = 0.42$ ppm for the resonances at 3.2 ppm, attributed to the piperazine protons (H_6–H_9). Likewise with **3** (Fig. S47†), a $\Delta\delta_H = 0.34$ ppm is observed on protonation. In D_2O, the $\Delta\delta_H$ is less subtle at 0.20 ppm. Otherwise, the crown ether protons (H_{13}–H_{22}) are negligibly shifted, and there is only a slight upfield $\Delta\delta_H$ for H_{10}–H_{12}, a slight downfield shift of the naphthalimide protons H_2 and H_4, and no change for naphthalimide protons H_1, H_3 and H_5. These results confirm protonation occurs at the aliphatic piperazine nitrogen atom.

Addition of Ba^{2+} to **4** in CD_3OD results in a downfield shift of 0.17–0.28 ppm for the crown ether protons H_{13}–H_{22} and broadening with loss of fine structure for the phenyl protons H_{10}–H_{12} (Fig. 5c). The crown ether proton signals are distorted, while the piperazine and naphthalimide proton signals are negligibly affected. Hence, the data indicates that binding of Ba^{2+} is restricted to the benzo-18-crown-6 ether. Addition of both D^+ and Ba^{2+} results in downfield shifts for all protons with the exception of naphthalimide protons H_1, H_3 and H_5, which become better resolved (Fig. 5d). The lack of any significant chemical shift for H_1, H_3 and H_5 suggests the carbonyl oxygen atoms do not assist with metal ion binding in the ground state.

A similar ^{1}H NMR analysis of **4** was performed in D_2O (Fig. S43†). The same three regions are clearly visible, although the aromatic region is more complex (Fig. S43a†). On addition of DCl, the resulting spectrum of **4**-D^+ is simplified and parallels the observations in CD_3OD (Fig. S43b†). The piperazine resonances for protons H_6–H_9 shift downfield $\Delta\delta_H = 0.20$ ppm and the crown ether protons H_{13}–H_{22} shift upfield by $\Delta\delta_H$ 0.28 ppm. In contrast, addition of Ba^{2+} results in a downfield shift of the crown ether protons by 0.1–0.2 ppm (Fig. S43c†). This result clearly demonstrates that **4** is perturbed by Ba^{2+} exclusively about the benzocrown in basic conditions. In the presence of both D^+ and Ba^{2+} (Fig. S43d†) the piperazine protons are downfield by $\Delta\delta_H = 0.4$ ppm, the crown ether protons are better resolved, and the benzocrown protons move upfield 0.20 ppm.

A ^{1}H NMR titration in D_2O was performed on **4** as a function of increasing aliquots of Ba^{2+} (Fig. S44†). All eight of the aromatic proton signals shift downfield by up to $\Delta\delta_H = 0.3$ ppm on addition of 10 equivalents of Ba^{2+}. The apparent triple at 7.0 ppm, assigned to overlapping H_2 and H_{11}, is resolved into two doublets on addition of 50 equivalents of Ba^{2+}. Similarly, ^{1}H NMR titration on **3** as a function of increasing aliquots of Na^+

(Fig. S46†) also shows a general downfield shift trend, which is most prominent at 100 equivalents (1200 mM). The piperazine protons H_{6-9} and the benzocrown protons H_{13-22} in conjunction with the phenyl protons H_{10-12} are electronically decoupled *via* the spacer units within the receptor$_1$–spacer$_1$–fluorophore–spacer$_2$–receptor$_2$ design and thus do not contribute to synergistic ^{1}H NMR chemical shifts.

Conclusions

A set of four 4-piperazino-*N*-aryl-1,8-naphthalimide molecular logic gates incorporating virtual C_0-type and ethylene (C_2-type) spacers, and benzocrown ether and piperazine moieties, were synthesised. Metal ion and proton binding constants were evaluated. We highlight that the benzo-18-crown-6 ether attached to the naphthalimide can capture Ba^{2+}. Furthermore, the crown-containing molecules were demonstrated as solvent-polarity fluorescent logic gates, specifically as two-input H^+, Na^+-driven or H^+, Ba^{2+}-driven TRANSFER gates in water, and two-input H^+, Na^+-driven and H^+, Ba^{2+}-driven AND gates in methanol, for the respective crown ethers. An interesting finding is that the *on* state of the benzo-15-crown-5 gate is brightest in methanol, while the benzo-18-crown-6 gate is brightest in 1 : 4 (v/v) water/methanol.

^{1}H NMR titration experiments were performed in D_2O and CD_3OD in order to examine the four logic (ground) states for the benzo-18-crown-6 logic gate. For the benzo-15-crown-5 logic gate, quality NMR spectra could only be obtain for the two states in acidic media due to limited solubility of the neutral compound at millimolar concentrations. These experiments nicely confirmed that the spacer units electronically decouple the fluorophore from the two receptors within the receptor$_1$–spacer$_1$–fluorophore–spacer$_2$–receptor$_2$ design. The NMR experiments also provide strong evidence for metal ion binding within the benzocrown cavity. However, there was no conclusive evidence for ground state interactions between a carbonyl of the naphthalimide and the metal ion within the benzocrown cavity. Therefore, the carbonyl oxygen atoms within the excited ICT fluorophore must be more basic in the excited state than in the ground state to account for the stronger metal ion binding interactions.[26]

These results should provide insight into the development of solvent-polarity reconfigurable fluorescent logic gates for probing the microenvironments at cellular membranes and protein interfaces.[10]

Experimental

A list of chemicals and instrumentation are provided in the ESI.† The syntheses of **1–4** are shown in Scheme 1.

General method for synthesis of 4-piperazino-*N*-aryl-1,8-naphthalimides

The 4-chloro-*N*-aryl-1,8-naphthalimide and excess piperazine (10–15 equivalents) were dissolved in 10 mL of DMF. The contents within the 50 mL round-bottom flask were heated and stirred at 130 °C until completion. The DMF was removed under vacuum by rotatory evaporator as an azeotropic mixture with heptane. The products were isolated by precipitation from a suitable solvent.

4-Piperazino-*N*-phenyl-1,8-naphthalimide (1)

4-Chloro-*N*-phenyl-1,8-naphthalimide (1.00 g, 3.25 mmol) and piperazine (3.46 g, 40.0 mmol) were reacted (general method). Addition of distilled cold water to the mixture gave an orange precipitate. The solid was collected by filtration and washed with cold distilled water and dried (1.07 g, 92% yield). R_f (9 : 1 (v/v) CH_2Cl_2/MeOH) = 0.88; m.p. 230 °C (dec.); ^{1}H-NMR (500 MHz, $CDCl_3$, ppm): δ 8.68 (dd, 1H, J = 7.3 Hz, 1.0 Hz, Naph-*H*), 8.60 (d, 1H, J = 8.0 Hz, Naph-*H*), 8.51 (dd, 1H, J = 8.5 Hz, 1.0 Hz, Naph-*H*), 7.81 (dd, 1H, J = 8.5 Hz, 7.3 Hz, Naph-*H*), 7.57 (m, 2H, Ph-*H*), 7.50 (m, 1H, Ph-*H*), 7.34 (m, 2H, Ph-*H*), 7.30 (d, 1H, J = 8.0 Hz, Naph-*H*), 3.93 (br, s, 2H, Pip-*H*), 3.76 (m, 2H, Pip-*H*), 3.33 (m, 2H, Pip-*H*), 3.28 (m, 2H, Pip-*H*); ^{13}C-NMR (125 MHz, $CDCl_3$, ppm): δ 40.21 (CH_2), 45.77 (CH_2), 52.72 (CH_2), 53.53 (CH_2), 115.73 (CH), 117.95 (C), 123.60 (C), 126.35 (C), 126.50 (CH), 128.70 (2CH), 129.36 (2CH), 129.97 (CH), 130.24 (C), 131.72 (CH), 132.75 (CH), 135.49 (C), 155.27 (C), 164.00 (CO), 164.48 (CO); IR ν_{max} (NaCl, cm^{-1}): 3064, 2906, 2831, 1699, 1653, 1560, 1507, 1369, 1232, 1004, 787, 740; HRMS (ES-TOF, m/z): calculated $C_{22}H_{20}N_3O_2$ 358.1556, found 358.1550.

4-Piperazino-*N*-(3,4-dimethoxyphenyl)-1,8-naphthalimide (2)

4-Chloro-*N*-(3,4-dimethoxyphenyl)-1,8-naphthalimide (500 mg, 1.36 mmol) and piperazine (1.53 g, 17.8 mmol) were reacted (general method). The orange solid was collected by filtration, washed with cold distilled water and dried (440 mg, 77% yield). R_f (9 : 1 (v/v) CH_2Cl_2/MeOH) = 0.90; m.p. 190 °C (dec.); ^{1}H-NMR (500 MHz, $CDCl_3$, ppm): δ 8.67 (dd, 1H, J = 7.2 Hz, 0.8 Hz, Naph-*H*), 8.58 (d, 1H, J = 8.0 Hz, Naph-*H*), 8.48 (dd, 1H, J = 8.5 Hz, 0.8 Hz, Naph-*H*), 7.79 (dd, 1H, J = 8.4 Hz, 7.4 Hz, Naph-*H*), 7.27 (d, 1H, J = 8.2 Hz, Naph-*H*), 7.02 (d, 1H, J = 8.5 Hz, Ph-*H*), 6.87 (dd, 1H, J = 8.4 Hz, 2.3 Hz, Ph-*H*), 6.80 (d, 1H, J = 2.3 Hz, Ph-*H*), 3.94 (s, 3H, –OC*H*$_3$), 3.91 (br, s, 2H, Pip-*H*), 3.88 (s, 3H, –OC*H*$_3$), 3.74 (m, 2H, Pip-*H*), 3.28 (m, 4H, Pip-*H*); ^{13}C-NMR (125 MHz, $CDCl_3$, ppm): δ 40.21 (CH_2), 45.77 (CH_2), 52.73 (CH_2), 53.52 (CH_2), 55.94 (–OCH_3), 56.05 (–OCH_3), 111.42 (CH), 111.78 (CH), 115.72 (CH), 117.95 (C), 120.76 (CH), 123.61 (C), 126.35 (CH), 128.16 (C), 129.98 (CH), 130.20 (C), 131.75 (CH), 132.78 (CH), 149.17 (C), 149.61 (C), 155.26 (C), 164.23 (CO), 164.71 (CO); IR ν_{max} (NaCl, cm^{-1}): 3008, 2929, 2835, 1705, 1662, 1585, 1512, 1436, 1369, 1238, 1002, 754; HRMS (ES-TOF, m/z): calculated $C_{24}H_{24}N_3O_4$ 418.1767, found 418.1752.

4-Piperazino-*N*-(benzo-15-crown-5)-1,8-naphthalimide (3)

4-Chloro-*N*-(benzo-15-crown-5)-1,8-naphthalimide (500 mg, 1.00 mmol) and piperazine (1.17 g, 13.5 mmol) were reacted (general method). The mixture was extracted using dichloromethane and water/triethylamine. The organic layer was collected and reduced under vacuum by rotary evaporator. Addition of cold acetone gave an orange precipitate. The solid was collected by filtration and washed with cold acetone and

diethyl ether and dried (520 mg, 94% yield). R_f (9 : 1 (v/v) CH_2Cl_2/MeOH) = 0.60; m.p. 246 °C (dec.); ^{1}H-NMR (500 MHz, $CDCl_3$, ppm): δ 8.66 (dd, 1H, J = 7.3 Hz, 1.1 Hz, Naph-*H*), 8.57 (d, 1H, J = 8.0 Hz, Naph-*H*), 8.47 (dd, 1H, J = 8.5 Hz, 1.1 Hz, Naph-*H*), 7.78 (dd, 1H, J = 8.4 Hz, 7.3 Hz, Naph-*H*), 7.27 (d, 1H, Naph-*H* overlapped by $CHCl_3$ residual speak), 7.00 (d, 1H, J = 8.5 Hz, Ph-*H*), 6.85 (dd, 1H, J = 8.5 Hz, 2.4 Hz, Ph-*H*), 6.80 (d, 1H, J = 2.4 Hz, Ph-*H*), 4.21 (m, 2H, Crown-*H*), 4.14 (m, 2H, Crown-*H*), 3.94 (m, 2H, Crown-*H*), 3.92 (br, s, 2H, Pip-*H*), 3.89 (m, 2H, Crown-*H*), 3.72–3.80 (m, 10H, Crown-*H*), 3.30 (m, 2H, Pip-*H*), 3.25 (m, 2H, Pip-*H*); ^{13}C-NMR (125 MHz, $CDCl_3$, ppm): δ 40.*22* (Pip-CH_2), 45.76 (Pip-CH_2), 52.72 (Pip-CH_2), 53.53 (Pip-CH_2), 69.22 (Crown-CH_2), 69.36 (Crown-CH_2), 69.59 (Crown-CH_2), 69.68 (Crown-CH_2), 70.68 (Crown-CH_2), 70.70 (Crown-CH_2), 71.23 (Crown-CH_2), 71.27 (Crown-CH_2), 114.19 (CH), 114.59 (CH), 115.72 (CH), 118.05 (C), 121.34 (CH), 123.67 (C), 126.32 (CH), 126.50 (C), 128.56 (C), 129.88 (CH), 130.20 (C), 131.69 (CH), 132.71 (CH), 149.33 (C), 149.71 (C), 155.19 (C), 164.09 (CO), 164.57 (CO); IR ν_{max} (NaCl, cm^{-1}): 3064, 2920, 2864, 1683, 1654, 1506, 1456, 1375, 1238, 1122, 1002, 771; HRMS (ES-TOF, m/z): calculated $C_{30}H_{34}N_3O_7$ 548.2397, found 548.2379.

4-Piperazino-*N*-(benzo-18-crown-6)-1,8-naphthalimide (4)

4-Chloro-*N*-(benzo-18-crown-6)-1,8-naphthalimide (203 mg, 3.70 mmol) and piperazine (408 mg, 4.86 mmol) were reacted (general method). Acetonitrile and diethyl ether were added to the solution mixture resulting in an orange precipitate. The solid was collected by filtration, and washed with cold diethyl ether and dried (175 mg, 81% yield). R_f (9 : 1 (v/v) CH_2Cl_2/MeOH) = 0.50; m.p. 240 °C (dec.); ^{1}H-NMR (500 MHz, $CDCl_3$, ppm): δ 8.61 (d, 1H, J = 7.2 Hz, Naph-*H*), 8.55 (d, 1H, J = 8.1 Hz, Naph-*H*), 8.47 (d, 1H, J = 8.5 Hz, Naph-*H*), 7.72 (t, 1H, J = 7.9 Hz, Naph-*H*), 7.24 (d, 1H, J = 8.1 Hz, Naph-*H*), 7.00 (d, 1H, J = 8.4 Hz, Ph-*H*), 6.85 (dd, 1H, J = 8.4 Hz, 2.1 Hz, Ph-*H*), 6.81 (d, 1H, J = 2.1 Hz, Ph-*H*), 4.22 (m, 2H, Crown-*H*), 4.16 (m, 2H, Crown-*H*), 3.95 (m, 2H, Crown-*H*), 3.90 (m, 2H, Crown-*H*), 3.71–3.79 (m, 12H, Crown-*H*), 3.27 (m, 4H, Pip-*H*), 3.22 (m, 4H, Pip-*H*), 2.95 (s, 2H, Pip-N*H*); ^{13}C-NMR (125 MHz, $CDCl_3$, ppm): δ 46.26 (2× Pip-CH_2), 54.40 (2× Pip-CH_2), 69.02 (Crown-CH_2), 69.18 (Crown-CH_2), 69.48 (Crown-CH_2), 69.57 (Crown-CH_2), 70.68 (Crown-CH_2), 70.72 (Crown-CH_2), 70.84 (2× Crown-CH_2), 70.90 (Crown-CH_2), 70.92 (Crown-CH_2), 113.87 (CH), 114.24 (CH), 115.02 (CH), 116.75 (C), 121.24 (CH), 123.44 (C), 125.70 (CH), 126.32 (C), 128.66 (C), 130.31 (C), 130.65 (CH), 131.51 (CH), 133.00 (CH), 148.93 (C), 149.71 (C), 156.65 (C), 164.31 (CO), 164.81 (CO); IR ν_{max} (NaCl, cm^{-1}): 3064, 2914, 1695, 1652, 1585, 1506, 1456, 1375, 1247, 1122, 945, 756; HRMS (ES-TOF, m/z): calculated $C_{32}H_{38}N_3O_8$ 592.2653, found 592.2657.

Author contributions

Conceptualization (DCM), investigation (GG), formal analysis (GG, DCM), supervision (DCM), writing – original draft (GG, DCM) and writing – review & editing (GG, DCM).

Conflicts of interest

There are no conflicts of interest to declare.

Acknowledgements

Financial support is acknowledged from the University of Malta. Prof. Robert M. Borg and Dr Duncan Micallef are thanked for NMR support.

References

1 (*a*) A. P. de Silva, *Molecular Logic-based Computation*, The Royal Society of Chemistry, Cambridge, UK, 2013; (*b*) K. Szaciłowski, *Infochemistry*, Wiley-VCH, Chichester, UK, 2012; (*c*) *Molecular and Supramolecular Information Processing: From Molecular Switches to Logic Systems*, ed. E. Katz, Wiley-VCH Verlag, Weinheim, Germany, 2012; (*d*) *Biomolecular Information Processing: From Logic Systems to Smart Sensors and Actuators*, ed. E. Katz, Wiley-VCH Verlag, Weinheim, Germany, 2012.

2 A. P. de Silva, H. Q. N. Gunaratne and C. P. McCoy, *Nature*, 1993, **364**, 42.

3 (*a*) B. Daly, J. Ling and A. P. de Silva, *Chem. Soc. Rev.*, 2015, **44**, 4203; (*b*) J. Ling, B. Daly, V. A. D. Silverson and A. P. de Silva, *Chem. Commun.*, 2015, **51**, 8403; (*c*) A. P. de Silva, T. S. Moody and G. D. Wright, *Analyst*, 2009, **134**, 2385; (*d*) D. C. Magri, *Analyst*, 2015, **140**, 7487.

4 (*a*) C.-Y. Yao, H.-Y. Lin, H. S. N. Cory and A. P. de Silva, *Mol. Syst. Des. Eng.*, 2020, **5**, 1325; (*b*) D. C. Magri, *Coord. Chem. Rev.*, 2021, **426**, 213598; (*c*) S. Erbas-Cakmak, T. Gunnlaugsson, S. Kolemen, T. D. James, A. C. Sedgwick, J. Yoon and E. U. Akkaya, *Chem. Soc. Rev.*, 2018, **47**, 2266; (*d*) J. Andréasson and U. Pischel, *Chem. Soc. Rev.*, 2018, **47**, 2228.

5 (*a*) G. J. Scerri, J. C. Spiteri, C. J. Mallia and D. C. Magri, *Chem. Commun.*, 2019, **55**, 4961; (*b*) J. M. A. Spiteri, C. J. Mallia, G. J. Scerri and D. C. Magri, *Org. Biomol. Chem.*, 2017, **15**, 10116; (*c*) D. C. Magri, M. Camilleri Fava and C. J. Mallia, *Chem. Commun.*, 2014, **50**, 1009; (*d*) D. C. Magri, G. J. Brown, G. D. McClean and A. P. de Silva, *J. Am. Chem. Soc.*, 2006, **128**, 4950.

6 (*a*) G. J. Scerri, J. C. Spiteri and D. C. Magri, *Mater. Adv.*, 2021, **2**, 434; (*b*) J. C. Spiteri, A. D. Johnson, S. A. Denisov, G. Jonusauskas, N. D. McClenaghan and D. C. Magri, *Dyes Pigm.*, 2018, **157**, 278; (*c*) J. C. Spiteri, S. A. Denisov, G. Jonusauskas, S. Klejna, K. Szaciłowski, N. D. McClenaghan and D. C. Magri, *Org. Biomol. Chem.*, 2018, **16**, 6195; (*d*) A. D. Johnson, K. A. Paterson, J. C. Spiteri, S. A. Denisov, G. Jonusauskas, A. Tron, N. D. McClenaghan and D. C. Magri, *New J. Chem.*, 2016, **40**, 9917; (*e*) J. C. Spiteri, J. S. Schembri and D. C. Magri, *New J. Chem.*, 2015, **39**, 3349; (*f*) T. J. Farrugia and D. C. Magri, *New J. Chem.*, 2013, **37**, 148.

7 (*a*) J. K. Tusa and H. He, *J. Mater. Chem.*, 2005, **15**, 2640; (*b*) H. He, M. A. Mortellaro, M. J. P. Leiner, S. T. Young, R. J. Fraatz and J. K. Tusa, *Anal. Chem.*, 2003, **75**, 549; (*c*)

T. Gunnlaugsson, M. Nieuwenhuyzen, L. Richard and V. Thoss, *J. Chem. Soc., Perkin Trans. 2*, 2002, 141; (*d*) T. Gunnlaugsson, M. Nieuwenhuyzen, L. Richard and V. Thoss, *Tetrahedron Lett.*, 2001, **42**, 4725; (*e*) T. Gunnlaugsson and J. P. Leonard, *Chem. Commun.*, 2003, 2424; (*f*) T. Konry and D. R. Walt, *J. Am. Chem. Soc.*, 2009, **131**, 13232; (*g*) S. Erbas-Cakmak, O. A. Bozdemir, Y. Cakmak and E. U. Akkaya, *Chem. Sci.*, 2013, **4**, 858.

8 (*a*) U. Reddy G, J. Axthelm, P. Hoffmann, N. Taye, S. Gläser, H. Görls, S. L. Hopkins, W. Plass, U. Neugebauer, S. Bonnet and A. Schiller, *J. Am. Chem. Soc.*, 2017, **139**, 4991; (*b*) V. Ramu, G. Upendar Reddy, J. Liu, P. Hoffmann, R. Sollapur, R. Wyrwa, S. Kupfer, C. Spielmann, S. Bonnet, U. Neugebauer and A. Schiller, *Chem.–Eur. J.*, 2019, **25**, 8453.

9 (*a*) N. Zerafa, M. Cini and D. C. Magri, *Mol. Syst. Des. Eng.*, 2021, **6**, 93; (*b*) M. E. S. West, C.-Y. Yao, G. Melaugh, K. Kawamoto, S. Uchiyama and A. P. de Silva, *Chem.–Eur. J.*, 2021, **27**, 13268; (*c*) M. Vella Refalo, N. V. Farrugia, A. D. Johnson, S. Klejna, K. Szacilowski and D. C. Magri, *J. Mater. Chem. C*, 2019, **7**, 15225; (*d*) C.-Y. Yao, J. Ling, L.-Y.-H. Chen and A. P. de Silva, *Chem. Sci.*, 2019, **10**, 2272; (*e*) A. P. de Silva, M. R. James, B. O. F. McKinney, D. A. Pears and S. M. Weir, *Nat. Mater.*, 2006, **5**, 787.

10 (*a*) C. Geraghty, C. Wynne and R. B. P. Elmes, *Coord. Chem. Rev.*, 2021, **437**, 213713; (*b*) W. Wang, J. Chen, H. Ma, W. Xing, N. Lv, B. Zhang, H. Xu and W. Wang, *Chem. Commun.*, 2021, **57**, 8166; (*c*) A. D. Johnson, J. A. Buhagiar and D. C. Magri, *RSC Med. Chem.*, 2021, **12**, 2060; (*d*) G. D. Wright, Y. Chao-Yi, T. S. Moody and A. P. de Silva, *Chem. Commun.*, 2020, **56**, 6838; (*e*) Y. Zhang, W. W. Chen, Y. Y. Fang, X. B. Zhang, Y. Liu and H. X. Ju, *J. Am. Chem. Soc.*, 2021, **143**, 15233; (*f*) B. McLaughlin, E. M. Surender, G. D. Wright, B. Daly and A. P. de Silva, *Chem. Commun.*, 2018, **54**, 1319.

11 (*a*) J. Ling, G. Naren, J. Kelly, T. S. Moody and A. P. de Silva, *J. Am. Chem. Soc.*, 2015, **137**, 3763; (*b*) J. Ling, G. Naren, J. Kelly, D. B. Fox and A. P. de Silva, *Chem. Sci.*, 2015, **6**, 4472.

12 A. P. de Silva, H. Q. N. Gunaratne and C. P. McCoy, *J. Am. Chem. Soc.*, 1997, **119**, 7891.

13 I. Johnson and M. T. Z. Spence, *The molecular probes handbook: a guide to fluorescent probes and labeling technologies*, 11th edn, 2010, Life Technologies Corporations, USA.

14 For example: A. P. de Silva, H. Q. N. Gunaratne, J. L. Habib-Jiwan, C. P. McCoy, T. E. Rice and J. P. Soumillion, *Angew. Chem., Int. Ed.*, 1995, **107**, 1728.

15 (*a*) S. Uchiyama, E. Fukatsu, G. D. McClean and A. P. de Silva, *Angew. Chem., Int. Ed.*, 2016, **55**, 768; (*b*) A. P. de Silva and K. R. A. S. Sandanayake, *Tetrahedron Lett.*, 1991, **32**, 421; (*c*) A. P. de Silva and K. R. A. S. Sandanayake, *J. Chem. Soc., Chem. Commun.*, 1989, 1183.

16 N. Jiang, J. Fan, F. Xu, X. Peng, H. Mu, J. Wang and X. Xiong, *Angew. Chem., Int. Ed.*, 2015, **54**, 1.

17 K. Pal, P. Kumar and A. Lal Koner, *J. Photochem. Photobiol., B*, 2020, **206**, 111848.

18 Reviews: (*a*) J. Li D. Yim, W. D. Jang and J. Yoon, *Chem. Soc. Rev.*, 2017, **46**, 2437; (*b*) P. A. Panchenko, O. A. Fedorova and Y. V. Fedorov, *Russ. Chem. Rev.*, 2014, **83**, 155; (*c*) G. W. Gokel, W. M. Leevy and M. E. Weber, *Chem. Rev.*, 2004, **104**, 2723; (*d*) G. W. Gokel, L. J. Barbour, R. Ferdani and J. Hu, *Acc. Chem. Res.*, 2002, **35**, 878; (*e*) G. W. Gokel, *Chem. Soc. Rev.*, 1992, **21**, 39.

19 Examples: (*a*) P. A. Panchenko Y. V. Fedorov, O. A. Fedorova and G. Jonusauskas, *Dyes Pigm.*, 2013, **98**, 347; (*b*) P. A. Panchenko, Y. V. Fedorov, O. A. Fedorova and G. Jonusauskas, *Phys. Chem. Chem. Phys.*, 2015, **17**, 22749; (*c*) P. A. Panchenko, Y. V. Fedorov, V. P. Perevalov, G. Jonusauskas and O. A. Fedorova, *J. Phys. Chem. A*, 2010, **114**, 4118; (*d*) P. A. Panchenko, Y. V. Fedorov and O. A. Fedorova, *J. Photochem. Photobiol., A*, 2018, **364**, 124; (*e*) P. A. Panchenko, A. S. Polyakova, Y. V. Fedorov and O. A. Fedorova, *Mendeleev Commun.*, 2019, **29**, 155; (*f*) C. Hou, A. M. Urbanec and H. Cao, *Tetrahedron Lett.*, 2011, **52**, 4903; (*g*) P. Nandhikonda, M. P. Begaye and M. D. Heagy, *Tetrahedron Lett.*, 2009, **50**, 2459; (*h*) G. W. Gokel, S. L. De Wall and E. S. Meadows, *Eur. J. Org. Chem.*, 2000, **17**, 2967.

20 Recent examples: (*a*) F. Nicoli M. Baroncini, S. Silvi, J. Groppi and A. Credi, *Org. Chem. Front.*, 2021, **8**, 5531; (*b*) Z. Liu, H. Zhang and J. Han, *Org. Biomol. Chem.*, 2021, **19**, 3287; (*c*) S. An, Q. Xu, Z. Ni, J. Hu, C. Peng, L. Zhai, Y. Guo and H. Liu, *Angew. Chem., Int. Ed.*, 2021, **60**, 9959.

21 (*a*) P. Thapa, I. Arnquist, N. Byrnes, A. A. Denisenko, F. W. Foss Jr, B. J. P. Jones, A. D. McDonald, D. R. Nygren and K. Woodruff, *Sci. Rep.*, 2019, **9**, 15097; (*b*) A. D. McDonald, *et al.*, *Phys. Chem. Lett.*, 2018, **120**, 132504; (*c*) N. Byrnes, F. W. Foss Jr, B. J. P. Jones, A. D. McDonald, D. R. Nygren, P. Thapa and A. Trinidad, *J. Phys.: Conf. Ser.*, 2019, **1312**, 012001.

22 I. Rivell, *et al.*, *Nature*, 2020, **583**, 48.

23 P. Thapa, N. K. Byrnes, A. A. Denisenko, J. X. Mao, A. D. McDonald, C. A. Newhouse, T. T. Vuong, K. Woodruff, K. Nam, D. R. Nygren, B. J. P. Jones and F. W. Foss Jr, *ACS Sens.*, 2021, **6**, 192.

24 (*a*) J. F. Callan, A. P. de Silva, J. Ferguson, A. J. M. Huxley and A. M. O'Brien, *Tetrahedron*, 2004, **60**, 11125; (*b*) D. P. Kennedy, C. D. Incarvito and S. C. Burdette, *Inorg. Chem.*, 2010, **49**, 916.

25 D. C. Magri, J. F. Callan, N. D. McClenaghan, A. P. de Silva, D. B. Fox and K. R. A. S. Sandanayake, *J. Fluoresc.*, 2005, **15**, 769.

26 A. Diacono, M. C. Aquilina, A. Calleja, G. Agius, G. Gauci, K. Szaciłowski and D. C. Magri, *Org. Biomol. Chem.*, 2020, **18**, 4773.

27 (*a*) R. K. Meka and M. D. Heagy, *J. Org. Chem.*, 2017, **82**, 12153; (*b*) P. Nandhikonda, M. P. Begaye, Z. Cao and M. D. Heagy, *Org. Biomol. Chem.*, 2010, **8**, 3195.

28 A. Weller, *Pure Appl. Chem.*, 1968, **16**, 115. E_{OX} is the oxidation potentials of 1,2-dimethoxybenzene (1.45 eV) or piperazine amine (1.15 eV), E_{RED} is the reduction potential of naphthalimide (−1.57 eV), E_S is the excited state singlet energy of naphthalimide (2.55 eV) and $e^2/\varepsilon r$ is the coulombic term (0.10 eV) where e is the electric charge of an electron, ε is the solvent dielectric constant and r the

separation distance. Potentials are versus SCE in acetonitrile.

29 W. Chi, J. Chen, Q. Qiao, Y. Gao, Z. Xub and X. Liu, *Phys. Chem. Chem. Phys.*, 2019, **21**, 16798.

30 L. N. Neupane, C. Raj Lohani, J. Kim and K.-H. Lee, *Tetrahedron*, 2013, **69**, 11057.

31 J. Hatai, S. Pal, G. P. Jose, T. Sengupta and S. Bandyopadhyay, *RSC Adv.*, 2012, **2**, 7033.

32 M. A. Cardona, M. Kveder, U. Baisch, M. R. Probert and D. C. Magri, *RSC Adv.*, 2016, **6**, 84712.